Experimental and Numerical Investigations of the Electro-Mechanical Response of Particle Filled Elastomers - Part II: Continuum Modeling Approach

Markus Mehnert, Jessica Faber, Mokarram Hossain, Shawn A. Chester and Paul Steinmann

Abstract A comprehensive experimental study performed under a combination of electro-mechanical loads on a particle-filled silicone as a representative of dielectric elastomers is presented in the Part I of this work (Mehnert et al., submitted, 2021). The constitutive modelling and numerical simulation of electro-active polymers are essential fields of research in order to increase the acceptance of this group of soft smart materials in real-life applications. However, only few contributions containing constitutive modelling approaches are combined with experimental data obtained from electro-mechanically coupled loading conditions due to the complexity of corresponding experiments. In this contribution, we aim to develop an electro-mechanically coupled model, which closely replicates the response of a silicone polymer filled with a high dielectric permittivity filler of varying fractions that are characterized under a combination of electric and mechanical loads. Once the model is calibrated with the experimental data described in Part I of this contribution, it is

Markus Mehnert
Institute of Applied Mechanics, University of Erlangen-Nuremberg, Egerlandstr. 5, 91058 Erlangen, Germany, e-mail: markus.mehnert@fau.de

Jessica Faber
Institute of Applied Mechanics, University of Erlangen-Nuremberg, Egerlandstr. 5, 91058 Erlangen, Germany, e-mail: jessica.faber@fau.de

Mokarram Hossain
Zienkiewicz Centre for Computational Engineering, College of Engineering, Bay Campus, Swansea University, Swansea, UK e-mail: mokarram.hossain@swansea.ac.uk

Shawn A. Chester
Mechanical & Industrial Engineering Department, New Jersey Institute of Technology, 200 Central Ave., Newark, NJ 07102, USA, e-mail: shawn.a.chester@njit.edu

Paul Steinmann
Institute of Applied Mechanics, University of Erlangen-Nuremberg, Egerlandstr. 5, 91058 Erlangen, Germany e-mail: paul.steinmann@fau.de
Glasgow Computational Engineering Centre (GCEC), University of Glasgow, United Kingdom

used for a simple illustrative application example showcasing the capability of the model and the influence of the different material characteristics.

1 Introduction

The term electro-active polymers (EAPs), defines a wide range of soft materials that have the ability of undergoing large deformations under excitation by an electric field [**?**]. This subclass of smart materials shows great potential as soft artificial muscles [**?**] thanks to their inherent mechanical properties. Furthermore, in various other potential applications such as stretchable sensors, flexible generators or flexible optics [**?, ?, ?, ?, ?, ?**], the use of EAPs shows great promise. Prominent examples of EAPs are the so-called dielectric elastomers (DEs) that are especially popular as they are relatively easy to manufacture and simple to handle. These can be used for the design of soft actuators by the addition of flexible electrodes on both sides of a thin polymeric layer. Upon the application of an electric potential difference between the electrodes, the sample contracts in the thickness direction while simultaneously expanding in the lateral directions due to the attractive forces between the oppositely charged electrodes. The extent to which an actuator will deform is determined by the mechanical and dielectric properties of the underlying soft polymer. While classical polymeric materials such as silicones or acrylates display necessary soft mechanical properties, these materials usually do not inherit specifically high dielectric constants and thus do not have favorable dielectric properties that are needed to induce the required forces from an externally applied electric field. A well-known concept for optimizing the dielectric properties is the addition of filler particles with high dielectric constant, such as Barium-Titanate, Titanium Oxides, carbon nanotubes, etc that enhance the overall electro-mechanical performances of the composites as demonstrated in Part I of this publication series.

In order to widen the applications and acceptance of EAP-based compounds, computational modeling approaches become indispensable tools in predicting the material response under a combined electro-mechanical loading. For predicting the purely mechanical response of particle filled polymeric materials, mathematical models used in computer-based simulations have been developed over the past years that were initially restricted to small deformations [**?**] and later extended accounting for large deformations based on finite strain theories, see [**?**]. Furthermore, in an effort to incorporate the rate-dependent behavior of particle filled polymers, various phenomenological models were developed using the concept of so-called stress-like internal variables for which suited evolution equations are required [**?, ?, ?**]. While these models considered the effective material as homogeneous, multiscale models such as [**?**] approached the topic by also investigating the behavior on the microscale, in which the particles and the polymeric base material can clearly be distinguished.

For developing mathematical models that can replicate electro-responsive material behavior, electro-mechanically coupled constitutive approaches were developed based on the interplay between a deforming body and an electric field, see the seminal works, e.g., by Eringen [**?**] or Toupin [**?**]. These ground-laying works have been expanded over the last decades especially sparked by the growing interests in electro-active soft polymeric materials [**?, ?, ?, ?**]. These concepts were also extended to so-called multiscale homogenization approaches, e.g. in the works by Keip et al. [**?, ?**] where two-scale homogenization methods are used for the solution of the electro-mechanical problem. Similarly, in a series of papers Lopez-Pamies et al. derived a homogenization method for dielectric composites capable of replicating the purely mechanical response of filled polymers and their electro-mechanical behavior [**?, ?, ?, ?, ?, ?**] validated by experimental data presented in [**?**]. In these works, special attention was put on the influence of particle interphases and the role of space charges on the material response.

Within the scope of the current work, we combine these concepts for the simulation of the electro-mechanical behavior of a particle filled silicone. To this end, a number of experiments were performed under electro-mechanical loads in order to characterize the material response of the silicone Elastosil P 7670$^{\text{TM}}$ filled with Barium-Titanate particles, see Part I of this publication series. Based on the obtained results, the material parameters of the presented model are identified resulting in a comprehensive constitutive model of the composite material under combined mechanical and electric loading.

This contribution is structured as follows. In Section 2 the general modeling approach is introduced. In the following Section, the experimental results and the modeling approach are combined in order to identify the necessary mechanical and electro-mechanical material parameters. In order to illustrate the material characteristics, a simple numerical application example is presented in Section 4. Finally, Section 5 presents a brief summary of this contribution and an outlook.
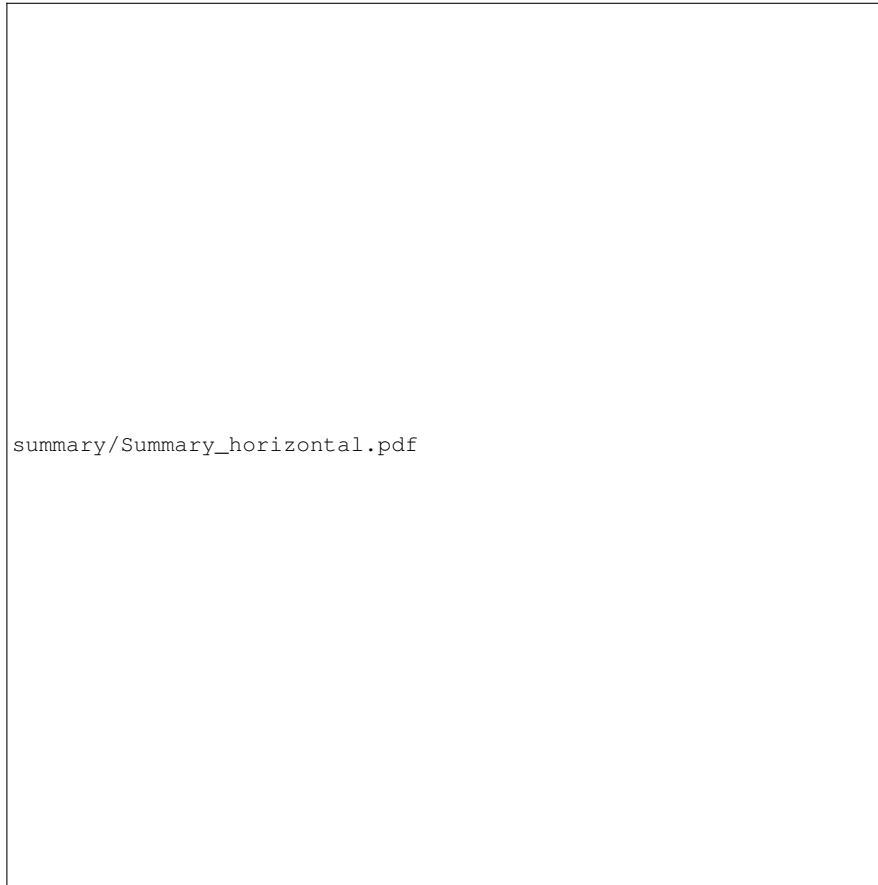
2 Constitutive modeling

In this section, an electro-mechanical modeling approach is presented and specified with suitable terms from the literature. The model is developed in such a way that the material behavior of both unfilled and particle filled silicones can be replicated as closely as possible with the experimental data produced in Part I of this contribution. Our prime aim is to reduce the number of material parameters appearing in the model to a minimum. However, the complexity of the observed responses results in an extensive format of the final expressions. As typical for other polymers, we assume that the underlying response of the unfilled silicone studied here is viscoelastic. However, by comparing the data obtained from the multistep relaxation tests and the cyclic loading tests with a very slow stretch rate ($\dot{\lambda} = 0.01 \text{ s}^{-1}$), we observe that there is a

rate-independent difference between the loading and the unloading curves. Furthermore, we can clearly identify a residual strain at the end of the deformation cycle. As the material samples were preconditioned, we do not consider this phenomenon as a consequence of the so-called Mullins effect, describing a unique and permanent softening of the material after the first deformation. Instead, we conjecture that in order to describe the observed material response, the classical elastic behavior has to be augmented to a pseudo-elastic material response as introduced in [**?**] , which has been used for the modeling of residual strains in different soft materials [**?**, **?**]. Therefore, this formulation is subsequently extended to viscoelasticity which captures the behavior of the base material. Such an approach is similar to the combination of viscoelasticity and stress-softening as presented by Wang and Chester [**?**]. The addition of filler particles alters both the elastic and viscous behavior, thus both energy contributions will be modified accordingly. Finally, the energy function has to be extended by electro-mechanical coupling terms that reflect the capability of the dielectric to deform under the application of an electric field. This combination of different material characteristics is summarized in Figure 1, showcasing the corresponding curves from the conducted experiments that characterize the specific material behavior.

Generally, we distinguish in our modeling approach between the response of the unfilled silicone (upper plots of Figure 1) and the particle filled compound (lower plots of Figure 1) where we assume that the unfilled material is the foundation that is subsequently extended. The underlying elastic material response of a pure silicone is modified to pseudo-elasticity in order to replicate the rate-independent hysteresis, visible in the upper central plot in Figure 1. Additionally, a rate-dependent response of the material is visible at increased strain rates as shown in the upper right plot. Consequently, the model is further extended to pseudo-viscoelasticity. Upon the addition of the stiffer particles, the material behavior noticeably changes. As shown in the plot on the lower left side, the underlying elasticity stiffens with the increasing particle concentration. This is accounted for by the modification of the elastic material model. Furthermore, the filler particles lead to an increase in the dissipated energy.Thus, the viscoelastic description of the material is modified. At this point, the mechanical response of the material is completed and this filler-content dependent pseudo-viscoelastic material model is extended to an electro-mechanically coupled form.

We assume the existence of an energy function W that can be used to derive the mechanical and electric quantities describing the material behavior. This energy function can be decomposed into a volumetric contribution W_{vol} and an isochoric contribution W_{iso}. The former describes the volume changing deformation whereas the latter describes the volume preserving part of the deformation. As we assume that the material under consideration shows incompressible response, the volumetric energy contribution vanishes and will not be addressed further in the following. Therefore, we can state that $W = W_{iso}$. Following the structure of the conducted

summary/Summary_horizontal.pdf

Fig. 1 A summary of the key structure of the different material characteristics under consideration.

experiments, we will extend and modify the expression stepwise to describe the material characteristics.

2.1 Constitutive modeling of the mechanical response of unfilled silicone

Initially, it is assumed that the energy function W consists of an elastic contribution W^{el} and a viscous contribution W^v. For modelling purely elastic response of a polymeric material, a wide range of well established energy functions can be found in the literature [**?**]. However, in the current case, a rate-independent hysteresis can be observed that would not be replicated by a strictly elastic approach. Consequently, a pseudo-elastic description is adopted from [**?**] resulting in an elastic energy contri-

bution that reads as

$$W^{el}(\overline{C}) = \eta_1 W_0^{el}(\overline{C}) + [1 - \eta_2] N(\overline{C}). \tag{1}$$

Here we introduce an elastic base function $W_0^{el}(\overline{C})$ that is formulated in terms of the isochoric part of the right Cauchy-Green tensor defined as $\overline{C} = J^{-2/3} F^T \cdot F$ with the deformation gradient F and its Jacobian $J = \det F$. In the current study, a Yeoh-type energy formulation is selected that reads

$$W_0^{el}(\overline{C}) = c_1^{el} \left[\overline{I}_1 - \dim \right] + c_2^{el} \left[\overline{I}_1 - \dim \right]^2 + c_3^{el} \left[\overline{I}_1 - \dim \right]^3 \tag{2}$$

For identifying the elastic material parameters c_i^{el} $(i = 1, 2, 3)$, experimental data obtained from the multistep relaxation tests of pure Elastosil will be used. Note that the first invariant of the right Cauchy-Green tensor is defined as $\overline{I}_1 = \overline{C} : I$, where I is the identity tensor. This base function is extended by the two parameters η_1 and η_2 as well as the function $N(\overline{C})$ that captures the rate-independent hysteresis and the residual strain. These parameters will be either active or inactive depending on the course of the deformations. While a sample material is loaded, it is assumed that $\eta_1 = 1$ and $\eta_2 = 1$, whereas they can take different values during unloading. We follow the notion given in [?] and define $N(\overline{C})$ as

$$N(\overline{C}) = \frac{1}{2} \left[v_1 \left[\overline{\lambda}_1^2 - 1 \right] + v_2 \left[\overline{\lambda}_2^2 - 1 \right] + v_3 \left[\overline{\lambda}_3^2 - 1 \right] \right] \tag{3}$$

which corresponds to a modified Neo-Hookean formulation with the material parameters v_i $(i = 1, 2, 3)$ and the principal isochoric stretches $\overline{\lambda}_i$. By the definition of the material parameters as

$$v_1 = \mu \left[1 - \frac{1}{3.5} \tanh(10[\lambda_m - 1]) \right],$$
$$v_2 = v_3 = \mu \tag{4}$$

the effect of a residual strain is introduced. The formulations contain a material parameter μ with a further dependency on the maximum strain λ_m in the loading direction. The parameters η_1 and η_2 from Equation (1) are defined as

$$\eta_1 = 1 - \frac{1}{r} \tanh\left(\frac{W_m^{el}(\overline{C}_m) - W_0^{el}(\overline{C})}{\mu m} \right),$$
$$\eta_2 = \tanh\left(\left[W_0^{el}(\overline{C}) / W_m^{el}(\overline{C}_m) \right]^{\alpha\left(W_m^{el}(\overline{C}_m) \right)} \right) / \tanh(1), \tag{5}$$
$$\alpha = a + b W_m^{el}(\overline{C}_m) / \mu,$$

where $W_m^{el}(\overline{C}_m)$ is the elastic energy at the maximum applied deformation $\overline{C}_m$ and the parameters r, m, a and b have to be identified using the results of the cyclic

loading experiments performed at the slowest stretch rate.

On the top of this, apparent changes in the stress-strain curve in response to a change in the deformation rate are attributed to a viscous contribution to the response of the unfilled material. Thus, the viscous contribution W^v is added to the energy function initially depending on the deformation described by the right Cauchy-Green tensor and a set of internal variables A_i, i.e.,

$$W^v(\overline{C}, A_i) = \sum_i W_i^v(\overline{C}, A_i). \tag{6}$$

In order to describe the complex time-dependent behavior of the material, the viscous energy consists of a number of functions $W_i^v(\overline{C}, A_i)$ ($i = 1, 2, 3...$), each of which represents a viscous Maxwell element. For the description of the response of pure Elastosil, we assume three viscous functions, the first two of which are defined as a Neo-Hookean type. In combination with the evolution equations that determine the internal variables, these read

$$W_i^v(\overline{C}, A_i) = \frac{1}{2} \sum_i \mu_i^v \left[\overline{I}_{1,i}^v - \dim \right],$$

$$\dot{A}_i = \frac{1}{\tau_i} \left[\overline{C} - \frac{1}{\dim} \overline{I}_{1,i}^v A_i \right], \tag{7}$$

with $i = 1, 2$. Here, the viscous shear moduli μ_i^v are introduced while the viscous invariants are defined as $\overline{I}_{1,i}^v = A_i^{-1} : \overline{C}$. The final contribution and its corresponding evolution law are formulated as a Yeoh-type function that reads

$$W_3^v(\overline{C}, A_3) = c_1^v \left[\overline{I}_{1,3}^v - \dim \right] + c_2^v \left[\overline{I}_{1,3}^v - \dim \right]^2 + c_3^v \left[\overline{I}_{1,3}^v - \dim \right]^3,$$

$$\dot{A}_3 = \left[\frac{1}{\tau_{3,1}} + \frac{2\left[\overline{I}_{1,3}^v - \dim \right]}{\tau_{3,2}} + \frac{3\left[\overline{I}_{1,3}^v - \dim \right]^2}{\tau_{3,3}} \right] \left[\overline{C} - \frac{1}{3} \overline{I}_{1,3}^v A_3 \right]. \tag{8}$$

It should be noted that the relaxation times $\tau_{3,i}$ ($i = 1, 2, 3$) are defined as $\tau_{3,i} = \tau_3/c_i^v$. These expressions are derived in a thermodynamically consistent way following the approach outlined in [?]. The viscous material parameters μ_i, c_i^v and τ_i ($i = 1, 2, 3$) have to be identified using the cyclic loading data obtained from tests performed at higher deformation rates.

2.2 Constitutive modeling of the mechanical response of particle filled silicone

As observed in the experimental data, the addition of filler particles leads to modifications of both the elastic and the viscous responses of the dielectric elastomers.

In the case of the elastic energy contribution $W^{el}(\overline{\boldsymbol{C}})$, these changes can be incorporated by introducing a modified invariant $\widetilde{I}_1^e$ following the approach presented in [**?**], which reads

$$\widetilde{I}_1^e = \left[1 + g_1^{el} v_f + \left[g_2^{el} v_f\right]^2\right]\left[\overline{I}_1 - \dim\right] + \dim = X_{el}\left[\overline{I}_1 - \dim\right] + \dim, \quad (9)$$

where v_f describes the filler content of the material and g_1^e and g_2^e are material parameters. The modified form of the elastic base energy from Equation (2) is labelled as $\widetilde{W}_0^{el}(\overline{\boldsymbol{C}})$ and reads

$$\widetilde{W}_0^{el}(\overline{\boldsymbol{C}}) = c_1^{el}\left[\widetilde{I}_1 - \dim\right] + c_2^{el}\left[\widetilde{I}_1 - \dim\right]^2 + c_3^{el}\left[\widetilde{I}_1 - \dim\right]^3. \quad (10)$$

Similar to the elastic part of the energy, the viscous contributions need modifications in order to capture the influence of the filler particles. The results of the cyclic loading tests show an increase in the stiffness of the material and a change in the form of the hysteresis curves originating from the addition of the fillers. Consequently, in addition to the introduction of a modified first invariant $\widetilde{I}_{1,i}^v$ $(i = 1, 2, 3)$ and material parameters g_1^v and g_2^v, a modification for each of the relaxation times τ_i $(i = 1, 2, 3)$ with a quadratic scaling function is introduced, i.e.,

$$\widetilde{I}_{1,i}^v = \left[1 + g_1^v v_f + \left[g_2^v v_f\right]^2\right]\left[\overline{I}_{1,i}^v - \dim\right] + \dim = X_v\left[\overline{I}_{1,i}^v - \dim\right] + \dim,$$

$$\widetilde{\tau}_i = \left[1 + g_{1,i}^\tau v_f + \left[g_{2,i}^\tau v_f\right]^2\right]\tau_i = X_{\tau,i}\tau_i. \quad (11)$$

It should be noted that the model parameters introduced here are responsible for the increase in the magnitude of the combined viscoelastic stress response and the amount of the energy dissipation. However, due to the complex interplay of the different Maxwell elements, a direct relation of each parameter to the form of the hysteresis is not possible. When these modifications are implemented into Equations (7) and (8), the first two member functions take the form

$$\widetilde{W}_i^v(\overline{\boldsymbol{C}}, \boldsymbol{A}_i) = 0.5 \sum_i \mu_i^v\left[\widetilde{I}_{1,i}^v - \dim\right],$$

$$\dot{\boldsymbol{A}}_i = \frac{1}{\widetilde{\tau}_i}\left[\overline{\boldsymbol{C}} - \frac{1}{\dim}\widetilde{I}_{1,i}^v \boldsymbol{A}_i\right], \quad (12)$$

whereas the final contribution reads

$$\widetilde{W}_3^v(\overline{\boldsymbol{C}}, \boldsymbol{A}_3) = c_1^v\left[\widetilde{I}_{1,3}^v - \dim\right] + c_2^v\left[\widetilde{I}_{1,3}^v - \dim\right]^2 + c_3^v\left[\widetilde{I}_{1,3}^v - \dim\right]^3,$$

$$\dot{\boldsymbol{A}}_3 = \left[\frac{1}{\widetilde{\tau}_{3,1}} + \frac{2\left[\widetilde{I}_{1,3}^v - \dim\right]}{\widetilde{\tau}_{3,2}} + \frac{3\left[\widetilde{I}_{1,3}^v - \dim\right]^2}{\widetilde{\tau}_{3,3}}\right]\left[\overline{\boldsymbol{C}} - \frac{1}{3}\widetilde{I}_{1,3}^v \boldsymbol{A}_3\right]. \quad (13)$$

In summary, the effect of the addition of filler particles on the mechanical response is modelled by eight modified parameters that have to be identified using the experimental results.

2.3 Constitutive modeling of the electro-mechanical response of particle filled silicone

Finally, coupling of the electric field with the mechanical response needs to be established. Within the data available in the current study, it is difficult to distinguish between the effects of the electric field on the elastic and the viscous parts of the material response. Hence, it is assumed that only the elastic energy contribution is dependent on the electric field. Such a simplification brings extra advantage as every additional electro-mechanical coupling parameter introduced here results in a considerable increase in the runtime of the optimization routine later on. Therefore, in order to keep the material parameters at a minimum, the electric coupling in the elastic energy contribution is introduced by modifications of the coupling invariant $\overline{I}_5$ and the dominating first material parameter c_1^e. Note that the viscous energy contributions are kept unchanged which renders the respective energy functions into the format

$$\widetilde{W}_0^{el}(\overline{\boldsymbol{C}}_{\text{EM}}, \mathbb{E}) = c_1^{el}(I_4)[\widetilde{I}_1 - \dim] + c_2^{el}[\widetilde{I}_1 - \dim]^2 + c_3^{el}[\widetilde{I}_1 - \dim]^3 + \gamma_2 \widetilde{I}_5. \tag{14}$$

Here we have introduced the fifth invariant $I_5 = [\mathbb{E} \otimes \mathbb{E}] : \overline{\boldsymbol{C}}$ that depends on the electric field that is defined as the material gradient of an electric potential φ as $\mathbb{E} = -\text{Grad}\varphi$. For a more detailed introduction of the electro-mechanical basics, reader is referred to [?, ?, ?, ?]. As is observed from the experimental data, the inclusion of filler particles increases the electro-mechanical coupling, hence, the field sensitive coupling parameters are modified via the particle concentration v_f in the form

$$c_1^{el}(I_4) = \hat{c}_1^{el} - [1 + kv_f]\beta^e I_4, \quad \gamma = [1 + kv_f]\hat{\gamma}, \tag{15}$$

where a fourth invariant $I_4 = [\mathbb{E} \otimes \mathbb{E}] : \boldsymbol{I}$ is introduced. The above equations convey the notion that the material has a zero field ground state captured by the parameter $\hat{c}_1$. This parameter is further influenced by the application of an electric field that can be scaled by the coupling parameters β^e and a factor k incorporating the concentration of the filler particles. Similarly, the coupling parameter γ_2 is also scaled by v_f in order to take into account the influence of increasing filler concentrations. Finally, in order to incorporate a field sensitivity of the elastic contribution, the pseudo-elasticity function $N(\overline{\boldsymbol{C}})$ is also modified into a field sensitive form. This is achieved by changing the material parameter μ introduced in Equation (4) into an expression $\widetilde{\mu}(I_4)$ that reads

$$\widetilde{\mu}(I_4) = \hat{\mu} - [1 + 5kv_f]\beta^e I_4. \tag{16}$$

Thus, three additional material parameters have to be identified using the results of the electro-mechanically coupled experiments in order to characterize the coupling behavior of the particle-filled silicone. Table 1 presents a summary of all 29 necessary material parameters appearing in the electro-mechanical modeling framework.

Elastosil P 7670™ filled with BaTiO$_3$ particles							
Mechanical Base Parameters							
Elastic Parameters							
$\hat{c}_1^{el}$			c_2^{el}			c_3^{el}	
Pseudo-Elastic Parameters							
$\hat{\mu}$		r	m		a		b
Viscous Parameters							
μ_1^v		μ_2^v	c_1^v		c_2^v		c_3^v
τ_1		τ_2			τ_3		
Particle Scaling Parameters							
Elastic Scaling Parameters							
g_1^e				g_2^e			
Viscous Scaling Parameters							
g_1^v	g_2^v	$g_{1,1}^\tau$	$g_{2,1}^\tau$	$g_{1,2}^\tau$	$g_{2,2}^\tau$	$g_{1,3}^\tau$	$g_{2,3}^\tau$
Electro-Mechanical Coupling Parameters							
β^e			$\hat{\gamma}_2$			k	

Table 1 A summary of the 29 material parameters of the modeling approach for Elastosil P 7670™ filled with BaTiO$_3$ particles. Parameters c_i, μ_i^v in N/mm^2, τ_i in s, β^e in N/(Vmm)^2, $\hat{\gamma}_2$ in N/V^2.

3 Parameter identification

In the following section, a material parameter identification process using the data obtained from the electro-mechanical experiments is described. This is done by calculating the resulting force over the course of a specific experiment and fitting this solution to the experimental results. We follow the same logic as in the previous chapter that proposes a modular structure of the constitutive framework. Consequently, the identification process starts by first finding the elastic, pseudo-elastic, and viscous material parameters of unfilled silicone, followed by the identification of the parameters describing the influence of the filler particles on the elastic and viscous material responses. In these cases, an analytical solution to the experiments can be calculated due to the selected sample geometry. Finally, the electro-mechanical coupling parameters are identified. However, due to the non-homogeneous sample deformation in these coupled experiments, the tests can not be assumed to be uniaxial and therefore, no analytical solution can be calculated. Thus, a numerical solution is obtained using a finite element implementation of the derived modeling approach

which is fitted to the experimental data.

For the identification of the mechanical parameters, the stress state during the conducted experiments can be calculated analytically. For this, we introduce the Piola-Kirchhoff stress tensor $\boldsymbol{S}$ as the derivative of the energy function with respect to the right Cauchy-Green tensor, i.e.,

$$S = 2\frac{\partial W(\overline{C}, A_i, \mathbb{E})}{\partial C}.$$

(17)

Here, the most general case is assumed considering that a particle filled silicone may be put under both mechanical and electric loads. In this context, it is usually convenient to introduce the isochoric version of the Piola-Kirchhoff tensor as $\overline{\boldsymbol{S}} = 2\partial W(\overline{C}, A_i, \mathbb{E})/\partial\overline{C}$ that we can transform into the conventional Piola-Kirchhoff stress $\boldsymbol{S}$ with the help of $\mathbb{P} = \partial\overline{C}/\partial C$, the fourth-order projection tensor. We can decompose this stress tensor further into an elastic part $\overline{\boldsymbol{S}}^{el}$ and a viscous part $\overline{\boldsymbol{S}}^{v}$. In order to compare these stresses to the obtained data curves, we introduce the Piola stress tensor $\boldsymbol{P}$ which is linked to $\boldsymbol{S}$ via

$$\boldsymbol{P} = \boldsymbol{F} \cdot [\overline{\boldsymbol{S}}^{el} + \overline{\boldsymbol{S}}^{v}] : \mathbb{P} = \boldsymbol{F} \cdot [\boldsymbol{S}^{el} + \boldsymbol{S}^{v}].$$

(18)

Following the classical assumption, the polymer studied here is considered as an incompressible material. Furthermore, for the case of purely mechanical experiments, the stress state inside a sample is homogeneous due to the selected sample geometry. Thus, the deformation gradient $\boldsymbol{F}$ and the corresponding right Cauchy-Green tensor $\boldsymbol{C}$ for the case of uniaxial stretching read

$$\boldsymbol{F} = \begin{bmatrix} \lambda & 0 & 0 \\ 0 & \lambda^{-1/2} & 0 \\ 0 & 0 & \lambda^{-1/2} \end{bmatrix}, \quad \boldsymbol{C} = \begin{bmatrix} \lambda^2 & 0 & 0 \\ 0 & \lambda^{-1} & 0 \\ 0 & 0 & \lambda^{-1} \end{bmatrix}.$$

(19)

Here, we define λ as $\lambda = [L_0 + \Delta L]/L_0$, the ratio between the extended length $L_0 + \Delta L$ and the initial length of the sample L_0. Consequently, the stretch rate is defined as $\dot{\lambda} = \overline{\Delta L}/L_0$. The stretch-like internal variables A_i take a form resembling $\boldsymbol{C}$, i.e.,

$$A_i = \begin{bmatrix} A_i^2 & 0 & 0 \\ 0 & A_i^{-1} & 0 \\ 0 & 0 & A_i^{-1} \end{bmatrix}.$$

(20)

In the following sections, this form of the deformation gradient is inserted into the definition of the stress in order to compare the experiments with the analytical solution.

3.1 Identification of the mechanical parameters of unfilled silicone

At first, the elastic base parameters c_i^{el} from Equation (2) are identified by fitting the analytical solution of the equilibrium curve to the corresponding experimental data. In this case, we assume that the recorded data can be attributed to the purely elastic material response. Thus, the analytical solution that is fitted to the experimental results reads

$$P^{el} = \frac{4}{3}\left[c_1^{el} + 2c_2^{el}\left[\lambda^2 + 2\lambda^{-1} - 3\right] + 3c_3^{el}\left[\lambda^2 + 2\lambda^{-1} - 3\right]^2\right]\left[\lambda - \lambda^{-2}\right]. \quad (21)$$

Note that in the aforementioned equation, the first elastic parameter is labelled as c_1^{el}. In the electro-mechanical case, where this term is scaled with the electric field, parameter c_1^{el} corresponds to the base parameter $\hat{c}_1^{el}$. For the purely mechanical case at present, however, the additional circumflex accent is omitted for the sake of readability. The fit of the analytical solution to the equilibrium curve is shown in Figure 2, with the identified material parameters $c_1^{el} = 0.0458\,\text{N/mm}^2$, $c_2^{el} = -0.0012$ N/mm^2 and $c_3^{el} = 9.9 \cdot 10^{-5}$ N/mm^2.
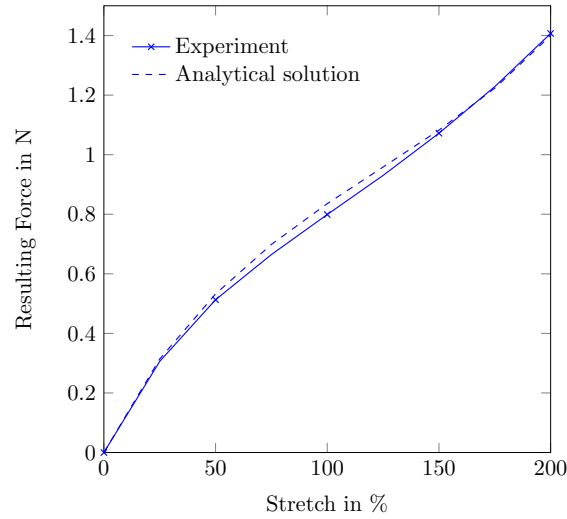

Fig. 2 Calibration of the analytical solution (dashed line) to the experimental results (solid line) of the resulting equilibrium force values obtained from a multi-step relaxation test of unfilled Elastosil P 7670$^{\text{TM}}$.

As was pointed out previously, the equilibrium curve corresponds to the loading path of the cyclic loading test with the slowest stretch rate ($\dot{\lambda} = 0.01$ s^{-1}). Thus, the unloading curve at this stretch rate is described by the additional terms in Equation

(1), i.e., the parameters μ, r and m from Equation (4) and (5). Consequently, the analytical solution that is fitted to the experimental results is modified to

$$P^{el} = \frac{4}{3}\eta_1 \left[c_1^{el} + 2c_2^{el} \left[\lambda^2 + 2\lambda^{-1} - \text{dim} \right] + 3c_3^{el} \left[\lambda^2 + 2\lambda^{-1} - \text{dim} \right]^2 \right] \left[\lambda - \lambda^{-2} \right]$$
$$+ \left[1 - \eta_2 \right] \left[v_1\lambda - 0.5[v_2 + v_3]\lambda^{-2} \right] \right].$$

$$(22)$$

The optimization of this solution to the respective cyclic loading data leads to the fit as presented in Figure 3 with the identified values $\mu = 1.5, r = 1.14$, and $m = 0.3427$.
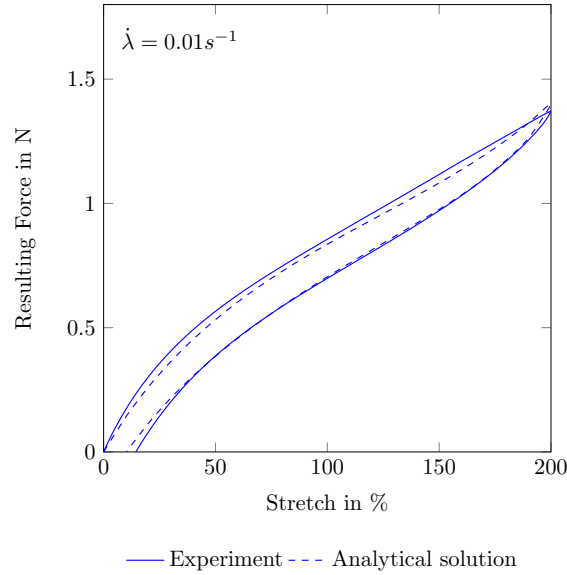
Fig. 3 Comparison between the experimental results (solid line) and the analytical solution (dashed) of cyclic loading-unloading tests performed with unfilled Elastosil P 7670$^{\text{TM}}$ with $\dot{\lambda} = 0.01$ s^{-1}. (Pseudo-elastic material behavior)

We can now use the already identified pseudo-elastic parameters as a basis for the identification of the viscous parameters. Thus, the viscous stress P^v originating from a Neo-Hookean type model in the stretch direction can be calculated as

$$P_i^v = \frac{4}{3}\mu_i^v \left[\lambda A_i^2 - \lambda^{-2} A_i^{-1} \right],$$
$$\dot{A}_i = \frac{1}{3\tau_i} \left[\lambda^2 A_i^{-1} - A_i^2 \lambda^{-1} \right] \quad \text{with } i = 1, 2.$$

$$(23)$$

However, Yeoh-type contribution takes the form

$$P_3^v = \frac{4}{3}\left[c_1^v + 2c_2^v\left[\overline{I}_{1,3}^v - 3\right] + 3c_3^v\left[\overline{I}_{1,3}^v - 3\right]^2\right]\left[\lambda A_3^{-2} - \lambda^{-2}A_3\right],$$

$$\dot{A}_3 = \left[\frac{1}{3\tau_{3,1}} + \frac{2}{3\tau_{3,2}}[\overline{I}_{1,3}^v - \dim] + \frac{1}{\tau_{3,3}}[\overline{I}_{1,3}^v - \dim]^2\right]\left[\lambda^2 A_3^{-1} - A_3^2\lambda^{-1}\right], \quad (24)$$

$$\text{with} \quad \overline{I}_{1,3}^v = \lambda^2 A_3^{-2} + 2\lambda^{-1}A_3,$$

The combination of the elastic and the viscous stresses can be fitted to multiple experimental data sets at the same time using a *simultaneous minimization* technique [**?**, **?**, **?**] in order to identify the viscous material parameters of the unfilled silicone. For this, the results of the experiments conducted with $\dot{\lambda} = 0.4$ s^{-1} and $\dot{\lambda} = 0.6$ s^{-1} are used as inputs for the optimization process, while the experimental data with the remaining stretch rates are used for the validation of the calibrated material parameters. Figure 4 shows the comparison between the experimental results and the model predictions with the identified material parameters summarized in Table 2.

μ_1^v	μ_2^v	c_1^v	c_2^v	c_3^v
$4.14 \cdot 10^{-3}$	$2.57 \cdot 10^{-3}$	$6.51 \cdot 10^{-3}$	$2.22 \cdot 10^{-14}$	$4.04 \cdot 10^{-6}$

τ_1	τ_2	τ_3
$4.39 \cdot 10^{-3}$	0.685	0.266

Table 2 Identified viscous material parameter sets for pure Elastosil P 7670$^{\text{TM}}$. μ_i^v, c_j^v in N/mm^2 and τ_i in s. Relaxation times τ_1 and τ_2 correspond to the Maxwell element modelled with a Neo-Hookean type formulation and the parameters μ_1^v and μ_2^v. Relaxation time τ_3 corresponds to the Maxwell element modelled with a Yeoh-type formulation and the parameters c_i^v.

The combination of viscous and pseudo-elastic material behavior captures the material response of the unfilled Elastosil silicone satisfyingly well.

3.2 Identification of the mechanical parameters of particle filled silicone

So far the material parameters for the unfilled silicone are identified as described step by step in the previous sections. Now, the parameters taking into account for the influences of the filler particles will be identified. For this, we derive the Piola stress in the stretching direction from Equation (10), which reads

$$P^{el} = \frac{4}{3}\left[X_{el}c_1^{el} + 2X_{el}^2 c_2^{el}[\lambda^2 + 2\lambda^{-1} - \dim] + 3X_{el}^3 c_3^{el}[\lambda^2 + 2\lambda^{-1} - \dim]^2\right]\left[\lambda - \lambda^{-2}\right].$$

with $X_{el} = 1 + g_1^{el}v_f + \left[g_1^{el}v_f\right]^2$

$$(25)$$

With this, the material parameters g_1^{el} and g_2^{el} are next identified by fitting the analytical solution to the equilibrium curves obtained from the multistep relaxation tests
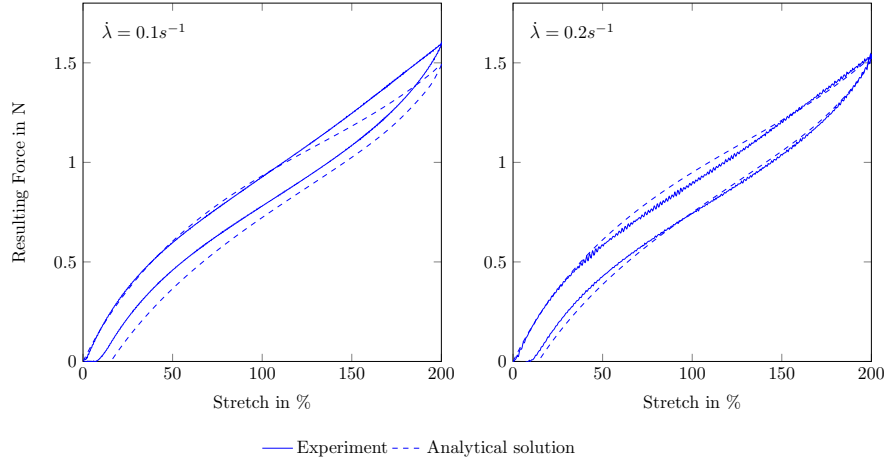
(a) Loading-unloading test with $\dot{\lambda} = 0.1$ s^{-1} and $\dot{\lambda} = 0.2$ s^{-1} used for the calibration of the model
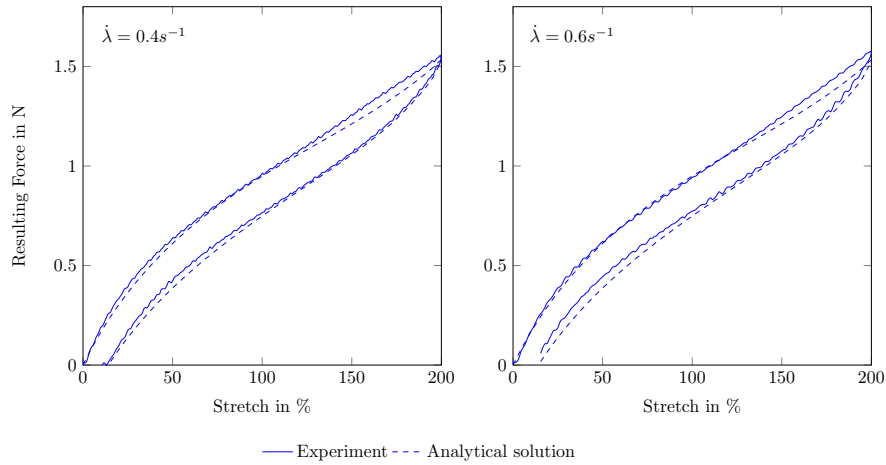
(b) Loading-unloading test with $\dot{\lambda} = 0.4$ s^{-1} and $\dot{\lambda} = 0.6$ s^{-1} used for the calibration of the model

Fig. 4 Comparison between the experimental results (solid lines) and the analytical solution (dashed lines) of cyclic loading-unloading tests performed with unfilled Elastosil P 7670$^{\text{TM}}$.

with different filler concentrations. The comparisons between the model predictions and the experimental data are depicted in Figure 5 for values $g_1^{el} = 2.81 \cdot 10^{-2}$ and $g_2^{el} = -1.323$.

In order to fully characterize the mechanical response of the filled silicone, we will now identify the remaining parameters that were introduced in Equation (11). To this end, the Neo-Hookean type viscous contributions of the Piola stress in the deformation direction are calculated as
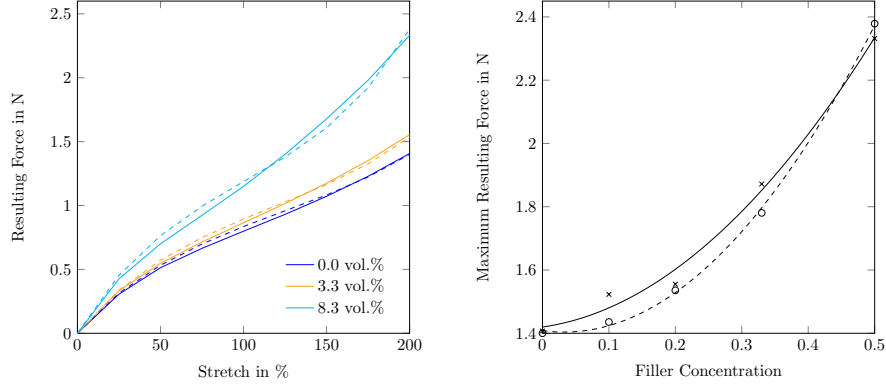
Fig. 5 Analytical solutions compared to experiments for the equilibrium values of the resulting force of multi-step relaxation tests for various filler concentrations. (Left) Analytical solution (dashed lines) and experimental values (solid lines) over the applied stretch, (right) simulation (o-marks and dashed trend line) and experimental values (x marks and solid line) of the resulting force for the maximum applied stretch over the range of tested filler concentrations.

$$
\begin{aligned}
P_i^v &= \frac{4}{3} X_v \mu_i^v \left[\lambda A_i^2 - \lambda^{-2} A_i^{-1} \right], \\
\dot{A}_i &= \frac{1}{3 X_{\tau,i} \tau_i} \left[\lambda^2 A_i^{-1} - A_i^2 \lambda^{-1} \right] \quad \text{with } i = 1, 2, \\
X_v &= 1 + g_1^v v_f + \left[g_2^v v_f \right]^2, \\
X_{\tau,i} &= 1 + g_{i,1}^\tau v_f + \left[g_{i,2}^\tau v_f \right]^2
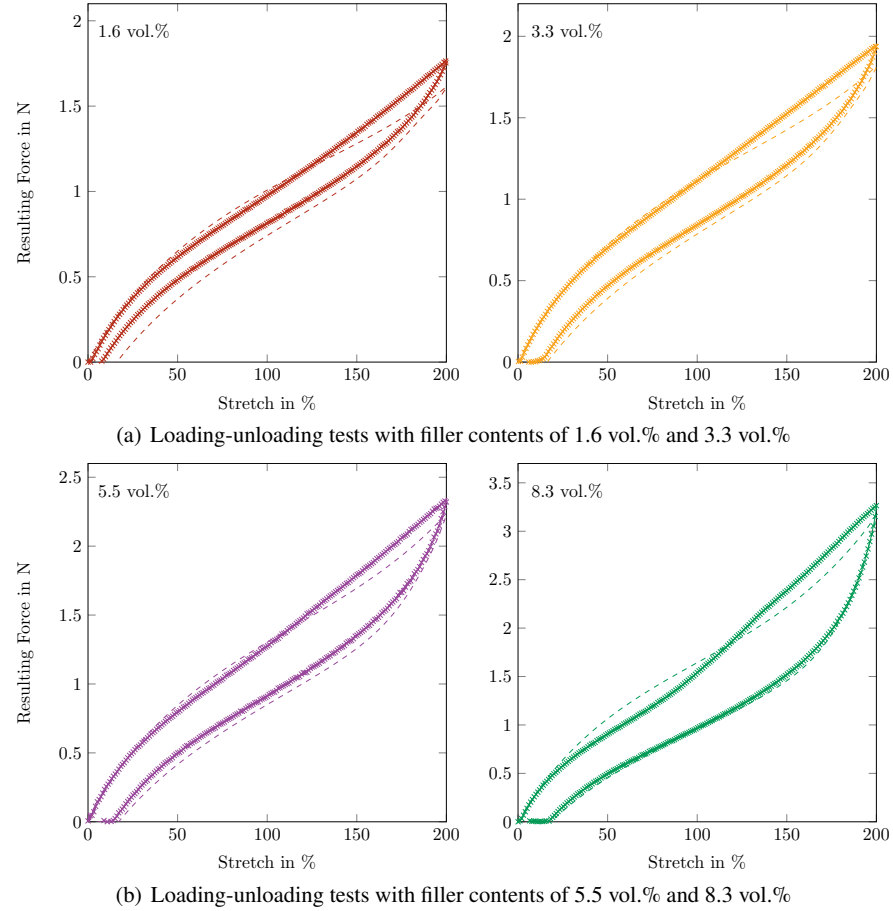\end{aligned}
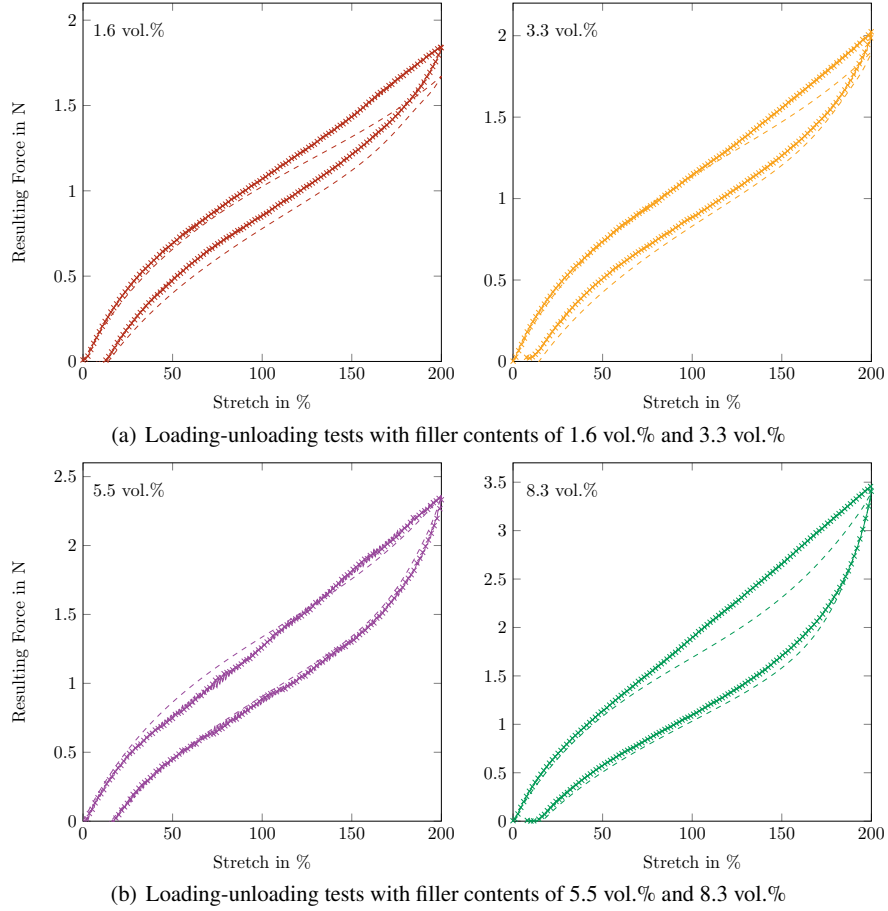\tag{26}
$$

while the Yeoh-type contributions take the form

$$
\begin{aligned}
P_3^v &= \frac{4}{3} \left[X_v c_1^v + 2 X_v^2 c_2^v \left[\overline{I}_{1,3}^v - 3 \right] + 3 X_v^3 c_3^v \left[\overline{I}_{1,3}^v - 3 \right]^2 \right] \left[\lambda A_3^{-2} - \lambda^{-2} A_3 \right], \\
\dot{A}_3 &= \left[\frac{1}{3 X_{\tau,3} \tau_{3,1}} + \frac{2}{3 X_{\tau,3} \tau_{3,2}} [\overline{I}_{1,3}^v - \dim] + \frac{1}{X_{\tau,3} \tau_{3,3}} [\overline{I}_{1,3}^v - \dim]^2 \right] \left[\lambda^2 A_3^{-1} - A_3^2 \lambda^{-1} \right], \\
\text{with} \quad \overline{I}_{1,3}^v &= \lambda^2 A_3^{-2} + 2 \lambda^{-1} A_3,
\end{aligned}
\tag{27}
$$

In combination with the previously derived stress contributions and the identified material parameters, this expression can be fit to multiple data sets of the cyclic loading experiments performed with various filler concentrations. Once again, a *simultaneous minimization* technique is used and the results of the experiments with 8.3 vol.% and 5.5 vol.% fillers at a stretch rate of 0.2 s^{-1} and 0.6 s^{-1} are used as input data for the optimization. This leads to a fit of the analytical solution to the experiments as presented in the Figures 6 to 9 while the identified material parameters as given in Table 3

g_1^v	g_2^v	$g_{1,1}^\tau$	$g_{2,1}^\tau$	$g_{1,2}^\tau$	$g_{2,2}^\tau$	$g_{1,3}^\tau$	$g_{2,3}^\tau$
4.267	0.405	−4.105	6.804	−4.105	6.804	6.794	1.081

Table 3 Identified viscous material parameters for filled Elastosil P 7670$^{\text{TM}}$.

(a) Loading-unloading tests with filler contents of 1.6 vol.% and 3.3 vol.%

(b) Loading-unloading tests with filler contents of 5.5 vol.% and 8.3 vol.%

Fig. 6 Comparison between the experimental results (x-marks) and the simulation (dashed lines) of cyclic loading-unloading experiments for Elastosil P 7670$^{\text{TM}}$ with various filler contents at a stretch rate of 0.1 s^{-1}.
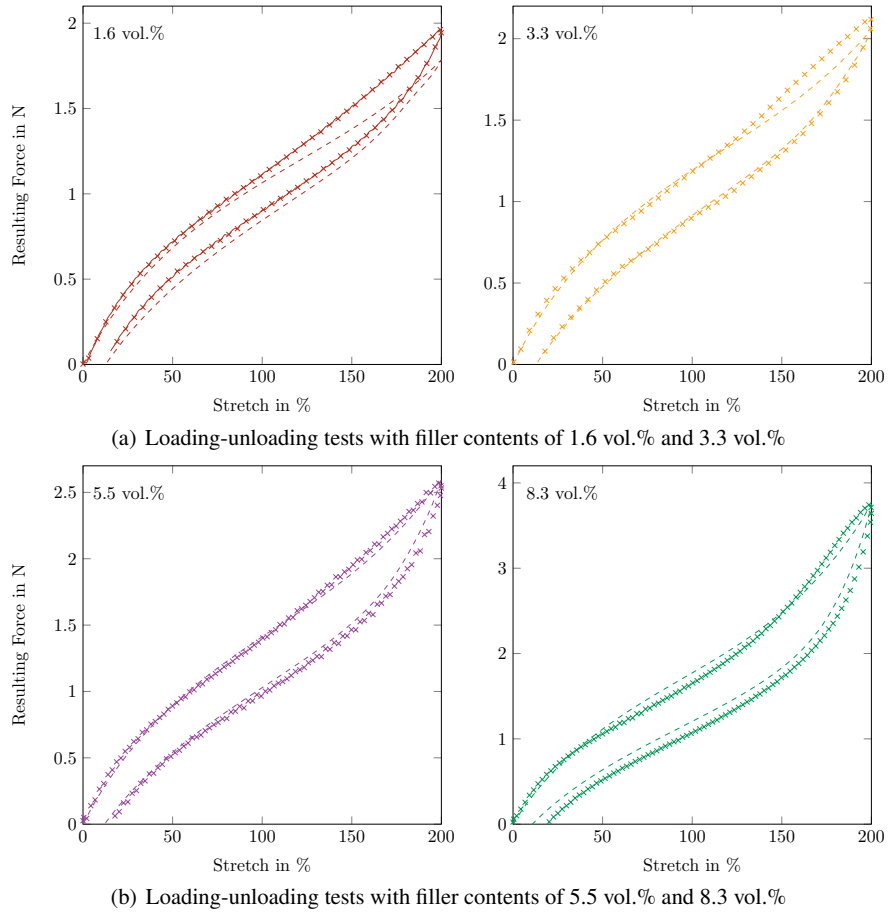
(a) Loading-unloading tests with filler contents of 1.6 vol.% and 3.3 vol.%

(b) Loading-unloading tests with filler contents of 5.5 vol.% and 8.3 vol.%

Fig. 7 Comparison between the experimental results (x-marks) and the simulation (dashed lines) of cyclic loading-unloading experiments for Elastosil P 7670$^{\text{TM}}$ with various filler content at a stretch rate of 0.2 s^{-1}.

3.3 Identification of the electro-mechanical coupling parameters of particle filled silicone

The identified mechanical parameters are now used as the basis for the characterization of the electro-mechanical coupling parameters. For electro-mechanical tests, the dimensions of the material samples have to be increased for the application of sufficient amount of electric field. Hence, it is not possible to find an analytical solution to the cyclic tests under an electro-mechanical load. Thus, the derived material model is implemented into a finite element code [?, ?, ?]. This numerical solution is then fitted to the experimental results in order to obtain the electro-mechanical coupling parameters γ, β^e and k. The resulting fit is shown in Figure 10 for the un-

(a) Loading-unloading tests with filler fractions of 1.6 vol.% and 3.3 vol.%

(b) Loading-unloading tests with filler fractions of 5.5 vol.% and 8.3 vol.%
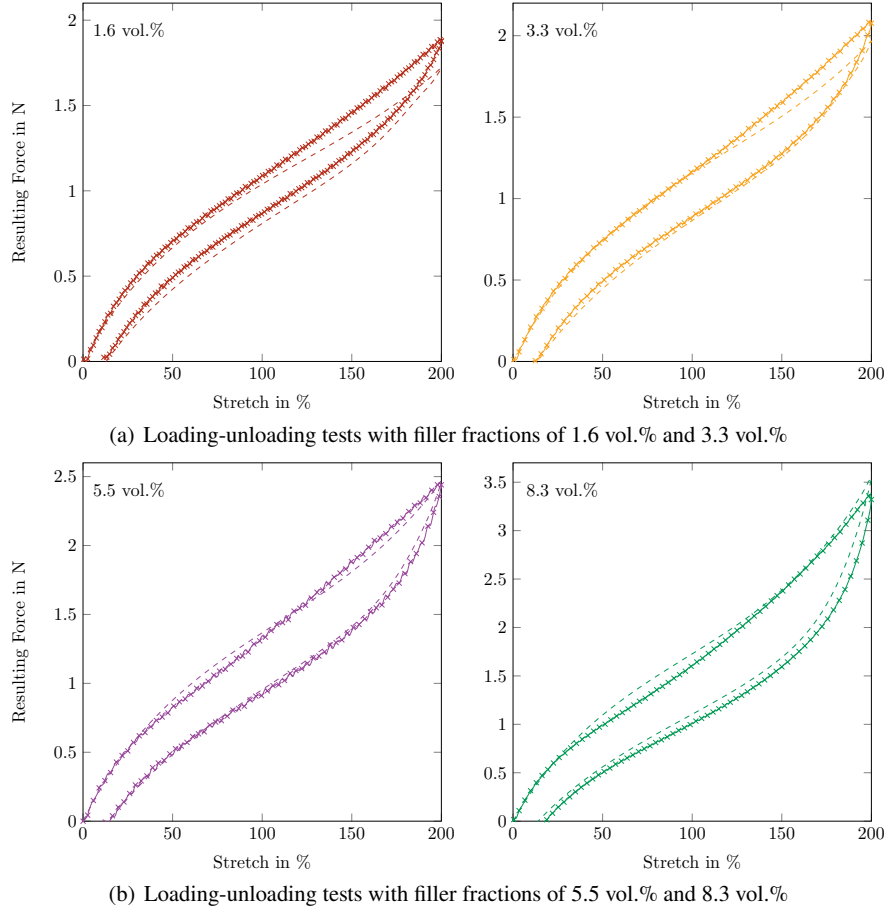
Fig. 8 Comparisons between the experimental results (x-marks) and the simulation (dashed lines) of cyclic loading-unloading experiments for Elastosil P 7670$^{\text{TM}}$ with various filler contents at a stretch rate of 0.4 s^{-1}.

filled silicone and Figure 11 for the particle filled material. The identified parameters are $\gamma = 4.41 \cdot 10^{-14}$, $\beta^e = 4.375 \cdot 10^{-13}$ and $k = 200$. The Figures show that the material model is capable of simulating the general material response of both pure silicone and the particle filled polymers. It should be emphasized that the response of this non-homogeneous experiment in the case that no electric potential difference is applied, relies solely on the material parameters identified earlier. Due to the increased complexity during the fabrication and the conduction of the experiments the simulation does not fit the experimental results as closely as in the uniaxial case presented in the previous sections. However, the quality of the fit is still satisfying and can therefore be considered as a validation of the purely mechanical material response. Considering the case that an electric field is applied during the experiments,

(a) Loading-unloading tests with filler contents of 1.6 vol.% and 3.3 vol.%

(b) Loading-unloading tests with filler contents of 5.5 vol.% and 8.3 vol.%
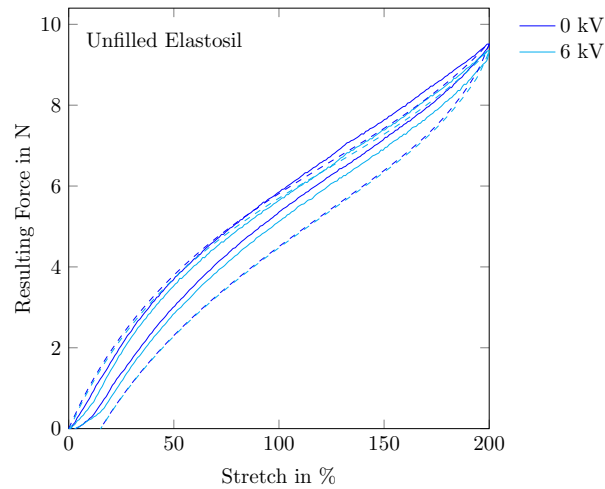
Fig. 9 Comparisons between the experimental results (x-marks) and the simulation (dashed lines) of cyclic loading-unloading experiments for Elastosil P 7670$^{\text{TM}}$ with various filler contents at a stretch rate of 0.6 s^{-1}.

it can be seen that the simulation still replicates the response of the material well. The identified values of the material parameters are summarized in Table 4.

4 Deformation of a Cylinder under Thermo-Electric Loading

As a simple yet illustrative numerical example, we present the deformation of a cylinder that is fixed in normal direction on one of its plane faces and loaded by an electric potential difference between the fixed and the opposing face, which results in a homogeneous deformation of the geometry. The purpose of this numerical in-

Fig. 10 Comparison between the experimental results (solid lines) and the simulation (dashed lines) of cyclic loading-unloading experiments with unfilled Elastosil and a stretch rate of 0.1s^{-1} with an applied electric voltage differences of 0 kV and 6 kV.
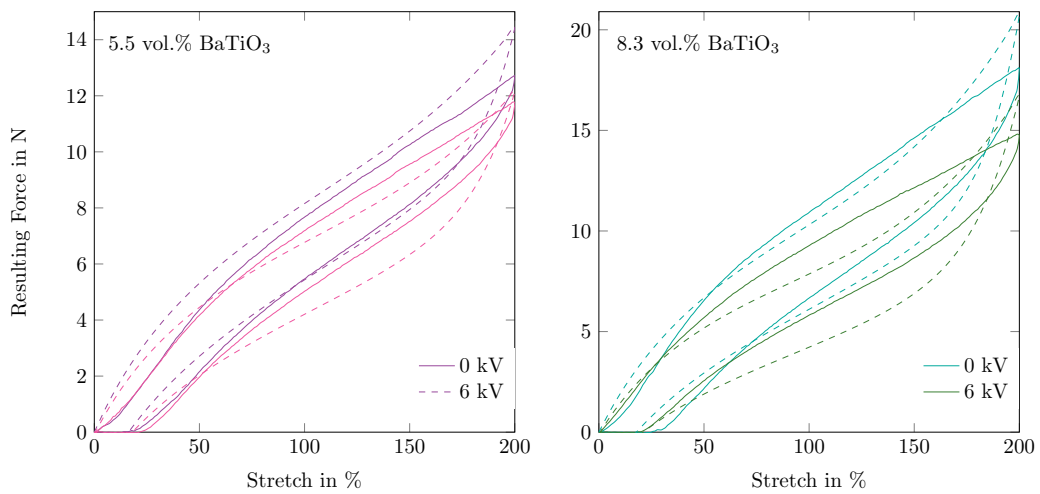
Fig. 11 Comparisons between the experimental results (solid lines) and the simulation (dashed lines) with Elastosil filled with (left) 5.5 vol.% BaTiO$_3$ and (right) 8.3 vol.% BaTiO$_3$ at a stretch rate of 0.1 s^{-1} for electric voltage differences of 0 kV and 6 kV.

vestigation is to present the effects of the electric field on the mechanical response of the viscous material. In contrast to the experiments presented in the preceding sections where the material response was dominated by the imposed mechanical deformation, the deformation of the cylinder is directly induced by the application of an electric field. These calculations are performed using the presented material

Elastosil P 7670$^{\text{TM}}$ filled with BaTiO$_3$ particles

Mechanical Base Parameters				
		Elastic Parameters		
$\hat{c}_1^{el}$		c_2^{el}		c_3^{el}
0.0458		-0.0012		$9.9 \cdot 10^{-5}$
		Pseudo-Elastic Parameters		
$\hat{\mu}$	r	m	a	b
0.45	1.14	0.3427	0.42	4.564
		Viscous Parameters		
μ_1^v	μ_2^v	c_1^v	c_2^v	c_3^v
$4.14 \cdot 10^{-3}$	$2.57 \cdot 10^{-3}$	$6.51 \cdot 10^{-3}$	$2.22 \cdot 10^{-14}$	$4.04 \cdot 10^{-6}$
τ_1	τ_2		τ_3	
$4.39 \cdot 10^{-3}$	0.685		0.266	

Particle Scaling Parameters							
			Elastic Scaling Parameters				
		g_1^{el}			g_2^{el}		
		$2.81 \cdot 10^{-2}$			-1.323		
			Viscous Scaling Parameters				
g_1^v	g_2^v	$g_{1,1}^\tau$	$g_{2,1}^\tau$	$g_{1,2}^\tau$	$g_{2,2}^\tau$	$g_{1,3}^\tau$	$g_{2,3}^\tau$
4.267	0.405	-4.105	6.804	-4.105	6.804	6.794	1.081

Electro-Mechanical Coupling Parameters		
β^e	γ	k
$4.375 \cdot 10^{-13}$	$4.41 \cdot 10^{-14}$	200

Table 4 Summary of the identified material parameters of the modeling approach for Elastosil P 7670$^{\text{TM}}$ filled with BaTiO$_3$ particles. Parameters c_i, μ_i^v in N/mm^2, τ_i in s, β^e in N/(Vmm)^2, γ in N/V^2.

model and the material parameters identified in the previous sections. In order to link this example to the experiments, the height of the investigated cylinder is 0.3 mm, as an approximation of the thickness of a material sample of Elastosil at the maximum deformation of 200 %. Furthermore, the potential difference applied between the plane faces of the cylinder is prescribed as 6 kV, which is the maximum potential difference applied in the experimental investigations. The potential difference is linearly increased over a specific ramp-up time t^{ramp} and is reduced back to zero over the same time to illustrate the viscous response of the material. The results are computed using the finite element implementation of the presented modeling approach. We assume that the geometry and the boundary conditions of the example are symmetric in relation to the center axis of the cylinder and the resulting deformation does not lead to a displacement of the material perpendicular to the cross section. Thus, the finite element model can be reduced to a quarter of the cross section of the cylinder in form of a two-dimensional mesh. This cross-section is a square with a side length of 0.15 mm and is discretized with 64 four-node elements. A sketch of the geometry with the prescribed boundary conditions and a plot of the simulated cross section of the cylinder in the deformed state is presented in Figure 12. It should be noted that as the resulting deformation is comparatively small, the result presented in the right

plot is scaled by a factor of 2 and the initial geometry of the cylinder is depicted with reduced opacity for the sake of visibility.

Figures/Num_Ex/Cube_sketch_deformation.pdf

Fig. 12 (left) A sketch of the model geometry with prescribed boundary conditions. (right) Resulting deformation of the cross section under thermo-electric loading for a ramp-up time of 10^3 s at reference temperature, deformation scaled by a factor of 2.

Now, a periodic loading of the cylinder is assumed such that in each cycle the magnitude of the electric potential difference is increased to the maximum value and then decreased to zero. The resulting normal displacement of the center of the top surface of the cylinder is depicted in Figure 13 for five cycles and various loading conditions.

The response of the cylinder illustrates both the effects of the addition of particles and the characteristics of the selected material model. Initially we will focus on the response of the unfilled silicone presented in the left plot of Figure 13. It can be seen that the cylinder does not return to its initial configuration after the first cycle

Figures/Num_Ex/Cube_cyclic_loading_silicone.pdf
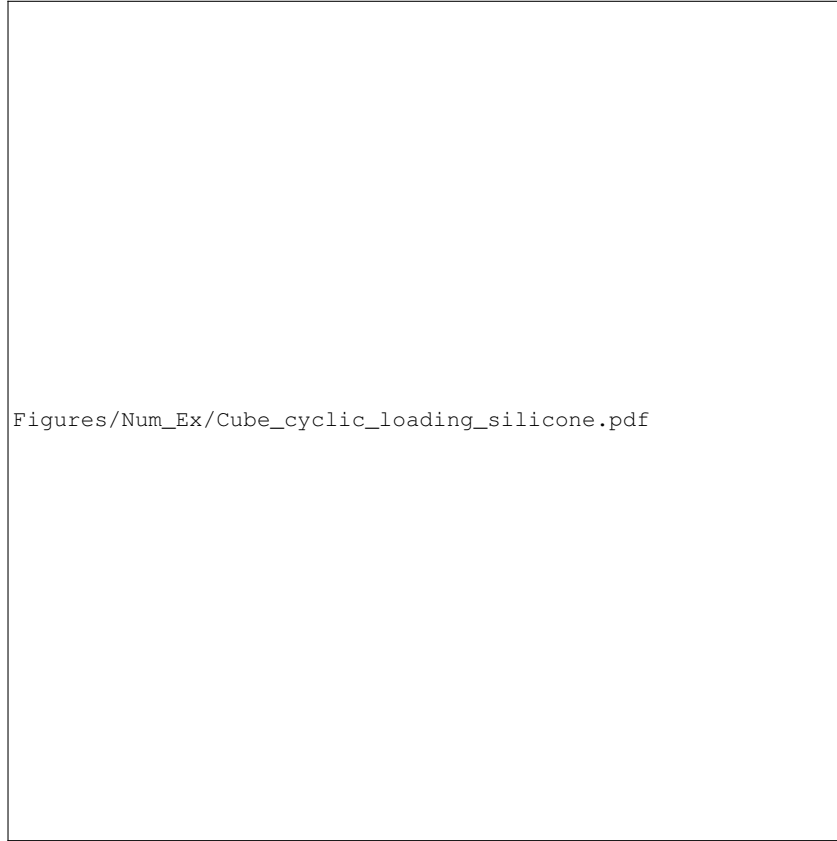
Fig. 13 Displacement of the center of the top surface of a cylinder of (left) pure Elastosil and (right) Elastosil filled with 8.3 vol.% BaTiO$_3$ particles for different ramp-up times of the electric field.

due to the viscous stress contributions. However, in the following cycles the cylinder returns almost exactly to the state at the beginning of the respective cycle, showing that the viscous characteristics of the unfilled material influence the overall response only slightly. This is emphasized even further by the fact that the ramp-up time has only a meager effect on the maximum displacement of the cylinder. When compared to the displacement of the filled material as shown in the right plot of Figure 13, it is clearly visible that the addition of particles with a high dielectric constant leads to a distinctly more pronounced displacement. As before, the cylinder does not return to its initial configuration after the end of the first cycle due to the viscous stress. However, now it can be seen that the viscous characteristics of the compound have a very distinct influence on the material response. First, the response is much more pronounced when the electric field is increased over a longer period of time as the elastic contributions are dominating the response. When the ramp-up time is reduced on the other hand, the displacement is reduced significantly as the viscous

contributions start to dominate the material response. Second, a close analysis of the displacement of the cylinder at the end of each cycle shows that this deformation increases with each cycle adding a viscous contribution to the deformation.

Taken together, for the application of this type of silicone, it is crucial to consider the desired rate of deformation. Even though the addition of $BaTiO_3$ particles leads to an increase of the effect of the electric field on the material, the resulting deformation is markedly dominated by the deformation rate and can drastically impact the realized deformation.

5 Conclusion and outlook

In this contribution, a numerical modeling approach for the simulation of particle filled dielectric elastomers under combined electro-mechanical loading was presented. The proposed model was specified for the viscoelastic silicone Elastosil P 7670$^{\text{TM}}$ filled with Barium-Titanate particles. In combination with the experimental results presented in Part I of this sequel, all relevant material parameters appearing in the constitutive model were identified here. For the replication of the mechanical experiments, analytical solutions were derived whereas in the case of an electro-mechanical load, the solution was calculated using an electro-mechanically coupled finite-element implementation. In our future work, we plan to combine the approach proposed herein with homogenization techniques in order to reduce the number of fitting parameters and analyze the interactions between the silicone and the filler particles in more detail similar to the recent studies shown in [**?**].